frontiers in Marine Science

ORIGINAL RESEARCH
published: 16 March 2022
doi: 10.3389/fmars.2022.835656

Wind-Controlled Transport of Saltwater in the Southeastern Baltic Sea: A Model Study

Victor Zhurbas[1] *and Germo Väli*[2]*

[1] Shirshov Institute of Oceanology, Russian Academy of Sciences, Moscow, Russia, [2] Department of Marine Systems, Tallinn University of Technology, Tallinn, Estonia

We hypothesized that the saltwater transport in a system of the southeastern Baltic basins including the Gdańsk and Gotland deeps connected by the Hoburg Channel, is greatly controlled by wind forcing, which has a clear physical explanation. Namely, the westerly winds develop the Ekman transport in the upper layer to the south from the Gotland Deep to the Gdańsk Deep which causes a compensatory saltwater countercurrent in the deep layer to the north from the Gdańsk Deep toward the Gotland Deep, and, vice versa, the easterly winds develop the Ekman transport to the north from the Gdańsk Deep toward the Gotland Deep causing a compensatory saltwater countercurrent in the deep layer to the south from the Gotland Deep to the Gdańsk Deep. To confirm the hypothesis, results of numerical modeling of the Baltic Sea circulation for a 10-year period (2010–2019) are applied. The daily saltwater transport to the northeast through a cross-section of the Hoburg Channel is found to be highly correlated with the wind stress component toward southeast (the correlation coefficient is 0.812) which can be considered as a straightforward confirmation of the hypothesis indicating the strong wind-driven circulation also in the deep layers of the Baltic Sea. Estimates of the daily saltwater transport through the above-mentioned and several other cross-sections of the southeastern Baltic Sea basins confirm a rule stating that the maximum correlation takes place between the saltwater transport and a wind stress component directed perpendicularly to the right relative to the direction of saltwater transport.

Keywords: Baltic Sea, wind-controlled saltwater transport, Ekman transport, compensatory flow, numerical modeling, GETM

OPEN ACCESS

Edited by:
William Savidge, University of Georgia, United States

Reviewed by:
Terry Whitledge, Retired, Fairbanks, Alaska, United States
Laura Tuomi, Finnish Meteorological Institute, Finland
Heiner Dietze, GEOMAR Helmholtz Center for Ocean Research Kiel, Helmholtz Association of German Research Centres (HZ), Germany

***Correspondence:**
Germo Väli
germo.vali@taltech.ee

Specialty section:
This article was submitted to Coastal Ocean Processes, a section of the journal Frontiers in Marine Science

Received: *14 December 2021*
Accepted: *24 February 2022*
Published: *16 March 2022*

Citation:
Zhurbas V and Väli G (2022) Wind-Controlled Transport of Saltwater in the Southeastern Baltic Sea: A Model Study. Front. Mar. Sci. 9:835656. doi: 10.3389/fmars.2022.835656

INTRODUCTION

The Baltic Sea is a semi-enclosed sea, the water exchange of which with the North Sea of the Atlantic Ocean is hampered by the presence of quite narrow and shallow straits—the Great and Little Belts and Öresund. The water balance of the Baltic Sea is made up of the inflow of saline water from the North Sea and the outflow of freshened water back, formed by mixing the incoming saline water with freshwater river runoff and precipitation. An overturning water-mass circulation in the Baltic Sea created in this way is referred to as the Baltic haline conveyor belt (Döös et al., 2004). As a result, the deep layer of the Baltic Sea below approx. 40–70 m depth is filled with saline water constituting

permanent halocline, and the only way to effectively ventilate it is by the lateral replacement with newly inflowing oxygenated saline water of the North Sea origin which is vital for the ecosystem functioning. Ventilation of the deepest layers of the Baltic Sea takes place only with very strong barotropic inflows called the Major Baltic Inflows (MBIs) which are quite rare and irregular (e.g., Matthäus and Frank, 1992; Mohrholz, 2018).

In fact, the Baltic Proper is a chain of basins connected by straits, and the depth of the basins and straits basically increases eastward and northward with distance from the transit area with the North Sea. The saline water of the North Sea origin spreads along the chain of basins and straits in the form of a bottom gravity current. An important link in this chain of basins is the Słupsk Furrow (SF), an elongated, channel-like topographic constriction between the Bornholm Basin in the west and the Eastern Gotland/Gdańsk basins in the east (**Figure 1**). The SF is the only pathway for saltwater of the North Sea origin to enter the deep basins of the eastern and northern Baltic Proper.

Keeping in mind the bottom topography (see **Figure 1**), the saltwater, leaving SF for the east, supposedly has two options to go. First, it can turn to the southeast toward the Gdańsk Basin and then, having made a cyclonic loop, rush north to the Gotland Deep through the Hoburg Channel. Second, it can turn to the northeast to rush directly to the Hoburg Channel and further enter the Gotland Deep. Which route is actually implemented is largely determined by dynamic processes in the bottom gravity currents. The first route (to the southeast to the Gdańsk Deep) is supported by the presence of a geostrophic balance of forces in the direction transverse to the gravitational current (e.g., Borenäs et al., 2007). Indeed, due to the geostrophic balance, the salty and dense water will flow eastward along the southern slope of SF and, after leaving it, will have to turn southeast and rush to the Gdańsk Deep along the southwestern slope of the basin. The second route (to the northeast directly to the Hoburg Channel and further to the Gotland Deep) is supposedly supported by a secondary circulation formed in a gravity current passing through a rotating channel (Johnson and Sanford, 1992). Namely, the Ekman transport to the north is formed in the bottom boundary layer beneath the eastward-flowing gravity current which moves the densest and saltiest water to the northern slope of SF (Zhurbas et al., 2012). As a result, the densest and saltiest water leaving SF gets a chance (at least a speculative one) to rush northeast directly to the Hoburg Channel.

In addition to the gravity current dynamics, the saltwater transport in the Baltic Sea is greatly influenced by the wind forcing. Numerical modeling of circulation in the Baltic Sea shows that the northerly and easterly winds promote transport of saltwater to the east in the lower layer of SF (Krauss and Brügge, 1991; Zhurbas et al., 2010, 2012). And vice versa, the southerly and westerly winds, promote a compensatory flow to the west in the lower layer of SF which weaken the eastward transport of saltwater, and, given a sufficiently strong southerly / westerly wind, can completely block it (Zhurbas et al., 2012).

Krauss and Brügge (1991) explained the above-mentioned feature of the wind-controlled saltwater transport through SF by a reasoning that the dominant wind-produced circulation is characterized by coastal jets in the wind direction and countercurrents in the central region, deflected by bottom topography. The water exchange between Bornholm and Eastern Gotland / Gdańsk basins occurs through SF, which is close to the center of the Baltic Sea at this longitude. Accordingly, bottom currents opposite to the wind direction prevail, which can explain the saltwater transport in SF to the east at easterly winds but cannot at northerly winds. However, in addition to the Krauss and Brügge (1991) explanation, one can hypothesize that the saltwater transport in SF to the east at northerly winds is caused by the wind-driven Ekman transport to the west in the upper layer which develops compensatory countercurrents in the lower layer.

Keeping in mind an analogy between the bottom topography configurations of the Bornholm Basin—SF—deep basins east of SF and the Gdańsk Deep—Hoburg Channel—Gotland Deep, one would expect that the easterly winds will contribute to the transport of saltwater coming from the SF to the southeast toward the Gdańsk Deep, and, vice versa, the westerly winds to the northeast toward the Hoburg Channel and Gotland Deep.

The objective of this study is to investigate the saltwater exchange between the basins of the southeastern Baltic Sea, including the Słupsk Furow, the Gdańsk Deep, the Hoburg Channel, and the Gotland Deep, depending on wind forcing based on multi-year numerical simulations and decide which effect, the wind-driven coastal jets or wind-driven Ekman transport in the open sea, prevails.

MATERIALS AND METHODS

Model Setup and Validation

The General Estuarine Transport Model (GETM; Burchard and Bolding, 2002) is applied to simulate thermohaline fields, salinity, currents, and overall dynamics in the southeastern Baltic Sea. GETM is a primitive equation, 3-dimensional, free surface, hydrostatic model with the embedded vertically adaptive coordinate scheme (Hofmeister et al., 2010; Gräwe et al., 2015; Klingbeil et al., 2018). The vertical mixing is parameterized by two equation k-ε turbulence model coupled with an algebraic second-moment closure (Burchard and Bolding, 2001; Canuto et al., 2001), and the implementation of the turbulence model is performed via General Ocean Turbulence Model (GOTM) (Umlauf and Burchard, 2005).

The model domain includes the entire Baltic Sea with an open boundary in the Kattegat (see **Figure 1A**) and has the horizontal grid spacing of 0.5 nautical miles (926 m) and 60 adaptive layers in the vertical direction. The digital topography of the Baltic Sea is obtained from the Baltic Sea Bathymetry Database.[1] The model run is started from 1 April 2010 with initial thermohaline conditions taken from the Baltic Sea reanalysis for the 1989–2015 by the Copernicus Marine service. The atmospheric forcing is adopted from HIRLAM (High Resolution Limited Area Model) version maintained by the Estonian Weather Service with the spatial resolution of 11 km (Männik and Merilain, 2007). For the lateral boundary conditions, time-series of observed sea

[1] http://data.bshc.pro/

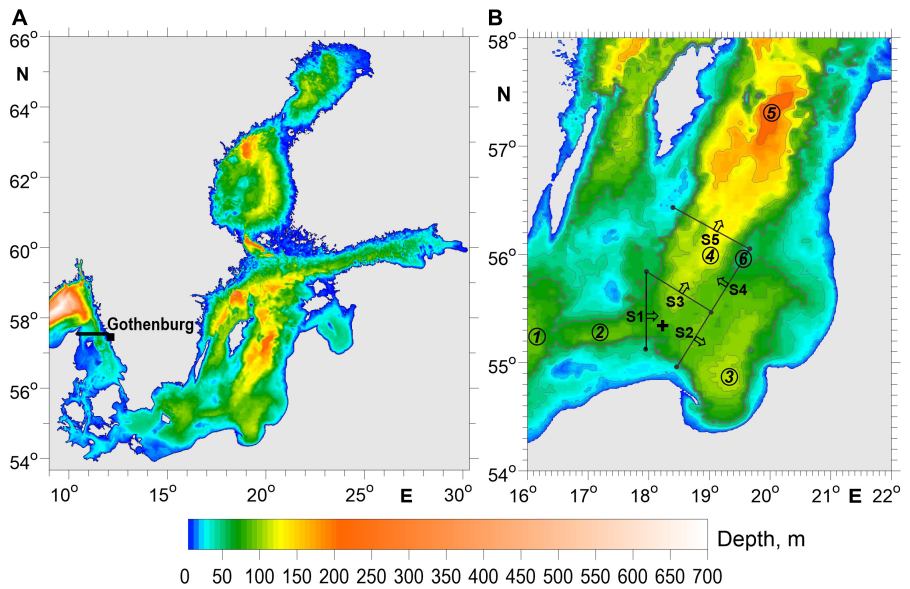

FIGURE 1 | (A) Bathymetric map of the Baltic Sea. The model domain has an open boundary close to Gothenburg (the bold black line). **(B)** Close-up of the southeastern Baltic Sea. The encircled numbers *1–6* point at the Bornholm Basin (*1*), the Słupsk Furrow (*2*), the Gdańsk Basin (*3*), the Hoburg Channel (*4*), the Gotland Deep (*5*), and the Klaipeda Bank (6). The black lines labeled S1–S5 are the locations of 5 cross-sections through which the saltwater transport is calculated. The arrows at the cross-sections show the direction corresponding to the positive value of the saltwater transport. The black cross points at the location of the IOW monitoring station TF0256.

surface height from Gothenburg Torshamnen coastal station and climatological profiles of temperature and salinity (Janssen et al., 1999) along the transect between Denmark and Sweden are used. More detailed information about the model setup is available in Zhurbas et al. (2018) and Liblik et al. (2020).

The model has been thoroughly tested by means of comparison of the simulated and observed current velocity variance and time series of sea-level fluctuations, temperature and salinity in the surface and bottom layers for a number of monitoring stations of the Baltic Sea including those of Bornholm and Gotland deeps (see Zhurbas et al., 2018 for details). Since this study is focused on the salt water transport in a transit area between the Bornholm, Gdańsk, and Gotland deeps where the salinity values in the permanent halocline are extremely variable, it seems reasonable to provide a specific, additional validation of the model based on the comparison of the measured and simulated bottom salinities in the area of interest. Time-series of salinity in the bottom and near-surface layers, measured at the IOW monitoring station TF0256 (18.246°E, 55.326°N), seem to be suitable empirical data for this purpose. This station is located at the eastern exit of the Słupsk Furrow where the saltwater pathway forks out into a southeastern branch toward the Gdańsk Deep and a northeastern branch toward the Gotland Deep (see **Figure 1**). Also we use for model validation the *in situ* salinity time-series in the permanent halocline of the Gotland Deep (monitoring station BY15, 100 m depth level). The time-series of salinity measured at TF0256 and BY15 during 10-year period of 2010–2019 show a reasonably good correspondence with the modeled time series in 2010–2017 and some positive bias of the modeled salinity in 2018–2019 (**Figure 2**).

Definition of the Saltwater Transport and Wind Stress

In order to characterize the saltwater transport in the transit area between the Bornholm, Gdańsk, and Gotland deeps, five cross-sections S1–S5 are chosen (see **Figure 1B**). The cross-sections are implied to be basically perpendicular to the sea depth contours while the saltwater flow in the deep / bottom layer follows basically the sea depth contours in view of topographic steering (e.g., Wåhlin, 2002). The cross-section chosen are:

- S1 is a cross cross-section through the SF outlet;
- S2+S4 is a transect from the Cape Rozewie, Poland, to the Klaipeda Bank, which is conditionally considered as the northwest boundary of the Gdańsk Basin;
- S2 is a cross-section through which the saltwater from SF supposedly enters the Gdańsk Basin;
- S3 is a cross-section through which the saltwater from SF supposedly goes directly to the Hoburg Chanel and further to the Gotland Deep;
- S4 is a cross-section through which the saltwater from SF having made a cyclonic loop in the Gdańsk Basin enters the Hoburg Channel;
- S5 is a cross cross-section though the Hoburg Channel.

Before calculating saltwater transport through cross-sections S1–S5, one has to define a salinity threshold dividing the freshened, upper layer water and the saltwater occupying the permanent halocline. Keeping in mind that the surface salinity in the area of interest is not constant but varies considerably (e.g., within 7.0–7.7 PSU for station TF0256 in accordance to

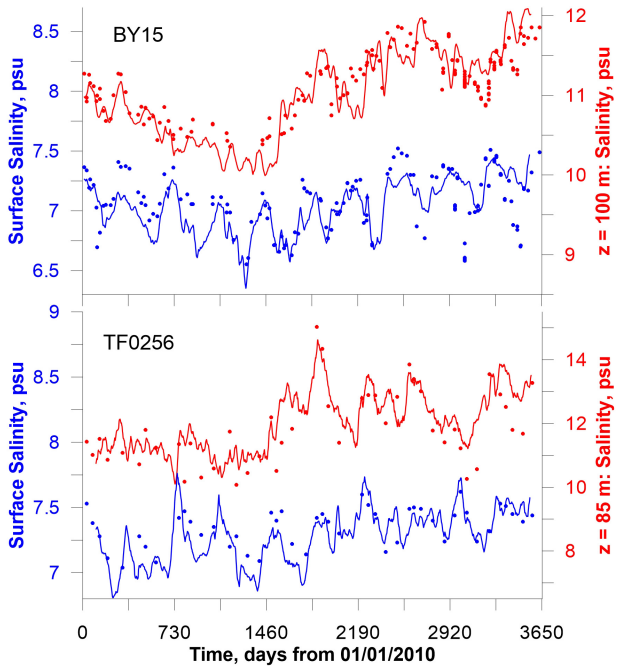

FIGURE 2 | Salinity time series at the sea surface (blue) and the permanent halocline / bottom layer (red) measured in the IOW monitoring station TF0256 (18.236°E, 55.326°N) and monitoring station BY15 in the Gotland Deep (dots) and simulated by the model (lines). The *in situ* data were taken from https://www.io-warnemuende.de/ (last access: 5 July 2021) and the Nest Institute's BED (Baltic Environmental Database) database.

Figure 2), we decided to choose for the salinity threshold not a constant value but a variable value which exceeds the surface salinity $S_{surface}$ by some constant surplus, namely by 1 PSU. Thus, we calculate saltwater transport through cross-section S1 (and similarly for S2–S5) as

$$T_{sal}(t) = \int_{S1}\int_{-H}^{0} S_{ex} u_N dz\, dl,\ S_{ex} = \begin{cases} S \text{ if } S \geq S_{surface} + 1 \\ 0 \text{ if } S < S_{surface} + 1 \end{cases}, \quad (1)$$

where S is salinity, H is the sea depth, dz and dl are increments along the vertical (z) axis and horizontally along the cross-section, respectively, u_N is the horizontal velocity component normal to the cross-section and positive in the direction shown by the arrows in **Figure 1**. Basically T_{sal} was calculated from the model output once a day using daily mean values of u_N, and, therefore, the T_{sal} time-series to be analyzed are the daily values of the saltwater transport.

Keeping in mind the goal to relate saltwater transports with the wind forcing, the proper parameter for the comparison seems to be the wind stress $\boldsymbol{\tau} = (\tau_x, \tau_y)$ rather than wind velocity at 10 m level $\boldsymbol{V}_{10} = (U_{10},\ V_{10})$. Indeed, the Ekman transport in the surface layer, T_E, is expressed as $T_E = |\boldsymbol{\tau}|/(\rho_0 f)$, where ρ_0 is the reference water density and f is the Coriolis parameter, and, therefore, the saltwater, transport being treated as compensatory flow in the bottom layer, is expected to depend linearly on the wind stress value $|\boldsymbol{\tau}|$.

To characterize effect of wind forcing on saltwater transport, the hourly time series of the 10-m level wind velocity from HIRLAM interpolated to the mid-point of cross-sections S1–S5 were used to calculate the wind stress time series as follows:

$$(\tau_x, \tau_y) = \rho_a c_D (U_{10}, V_{10}) |\boldsymbol{V}_{10}|, \quad (2)$$

where $\rho_a = 1.28\ \text{kg}\cdot\text{m}^{-3}$ is the air density and c_D is the drag coefficient which can be found from the empirical formula (Large and Pond, 1981).

$$c_D = 1 \cdot 10^{-3} \begin{cases} 1.14 \text{ at } |\boldsymbol{V}_{10}| < 10\ \text{m}\cdot\text{s}^{-1} \\ 0.49 + 0.065 \cdot |\boldsymbol{V}_{10}| \text{ at } |\boldsymbol{V}_{10}| \geq 10\ \text{m}\cdot\text{s}^{-1} \end{cases}. \quad (3)$$

Further, the arithmetic average of 24 consecutive terms of the hourly series of $\boldsymbol{\tau}$ was found to obtain a time series of daily mean values of the wind stress, $\langle\boldsymbol{\tau}\rangle$.

Note that the GETM model uses a more advanced parameterization of momentum flux through the air-sea interface which is based on a wider set of input parameters including U_{10}, V_{10}, precipitation, sea surface temperature, as well as temperature, pressure and humidity of the air (Kondo, 1975). We prefer to use a simple formulation such as Eq. (2)–(3) because it is easier to implement due to the fact that it is based on wind data alone.

RESULTS

The wind driven Ekman transport in a relatively deep, open sea, $T_E = |\boldsymbol{\tau}|/(\rho_0 f)$, is proportional to the wind stress and directed perpendicularly to the right (in the Northern Hemisphere) from the direction of the wind (and the direction of wind stress defined by Eq. 2–3). Therefore, in order to statistically access the azimuthal distribution and the most probable direction of the Ekman transport, we calculated the distribution of the cumulative wind stress (in percent) for a 10-year period (2010–2019) depending on the wind vector direction (**Figure 3**).

The azimuthal distribution of the wind stress is found to be strongly anisotropic with 45% of the total within a narrow range of the wind velocity vector angle [0°, 60°] (the angle is counted counterclockwise from the east). Therefore, 45% of the total wind-driven Ekman transport in the southeastern Baltic Sea goes to the south-southeast within the angle range [–90°, –30°]. We do not present the distribution of the cumulative wind stress depending on the direction of the wind velocity vector for sections S2–S5, since it is similar to that for section S1 shown in **Figure 3**. This is not surprising, since all sections S1–S5 are located in the open sea at a distance of no more than 100 km, which is not large enough to provide significant differences in long-term wind statistics.

In accordance to our hypothesis presented in the Abstract and Introduction, the saltwater transport though SF is expected to be negatively correlated with the y-component of the wind stress τ_y defined by Eq. (2). This expectation is clearly confirmed by **Figure 4** where a scatter plot of the daily saltwater transport T_{sal} through cross-section S1 vs. the daily mean of the y-component of the normalized wind stress $\langle\tau_y/\rho_0\rangle$ is presented.

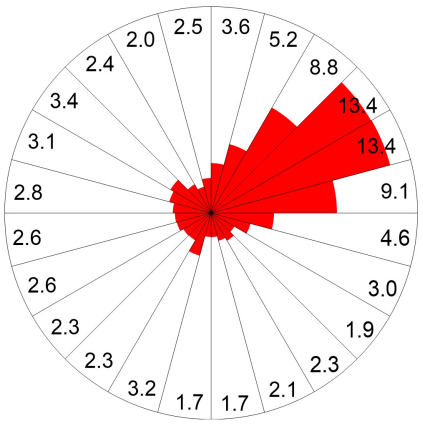

FIGURE 3 | Distribution of the cumulative wind stress (in percent) in the mid-point of cross-section S1 for a 10-year period (2010–2019) depending on direction of the wind velocity vector.

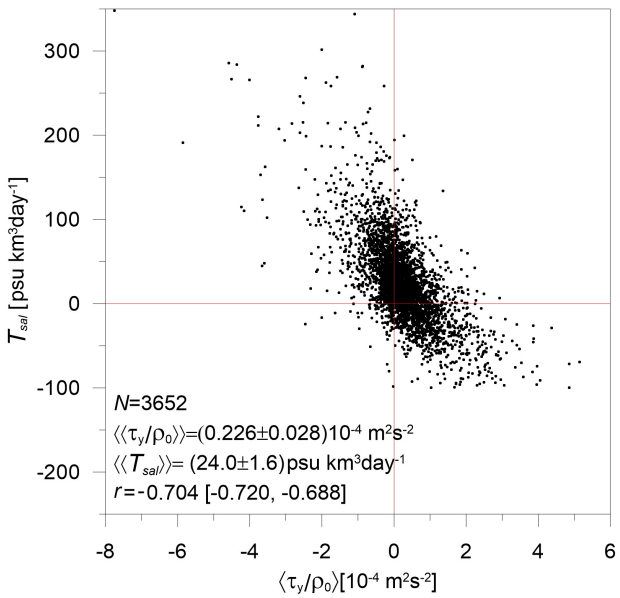

FIGURE 4 | A scatter plot of the daily saltwater transport T_{sal} through cross-section S1 vs. the daily mean of the y-component of wind stress $\langle\tau_y/\rho_0\rangle$; $\langle\langle\ldots\rangle\rangle$ is the 10-year mean value. The numbers in the square brackets and next to the ± sign quantify the 95% confidence limits.

The correlation coefficient for the 10-year time series of T_{sal} and $\langle\tau_y/\rho_0\rangle$ is $r = 0.704$. Note that the 10-year mean values of $\langle\tau_y/\rho_0\rangle$ and T_S are $\langle\langle\tau_y/\rho_0\rangle\rangle = (0.226 \pm 0.028)\cdot10^{-4}$ m^{2}s^{-2} (which confirms the prevalence of southerly winds in accordance to **Figure 3**) and $\langle\langle T_{sal}\rangle\rangle = 24.5 \pm 1.6$ psu·km^{3}day^{-1} (which corresponds to the transport of salt water to the east through the SF on average).

To obtain statistical estimates of saltwater transport through cross-sections S1–S5 depending on the wind force and wind direction, a partial mean $\langle T_{sal}\rangle$ of the daily saltwater transport T_{sal} was calculated for 12 ranges of the wind vector direction and 4 ranges of the daily mean friction velocity $u_* = \sqrt{\langle\tau_x/\rho_0\rangle^2 + \langle\tau_y/\rho_0\rangle^2}$ based on the 10-year time series (**Figure 5**).

At light to moderate winds of any direction, the partial mean saltwater transport $\langle T_{sal}\rangle$ through cross-section S1 (i.e., through SF) remains positive (eastward) being maximum for winds blowing to the south and minimum for winds to the north. For strong winds blowing to the north, the $\langle T_{sal}\rangle$ through S1 has reversed to the west (becomes negative). If the wind increases to stormy, then the reverse transport of saltwater to the west in SF becomes stronger and takes place in a wider range of wind vector angle from 0 to 150°.

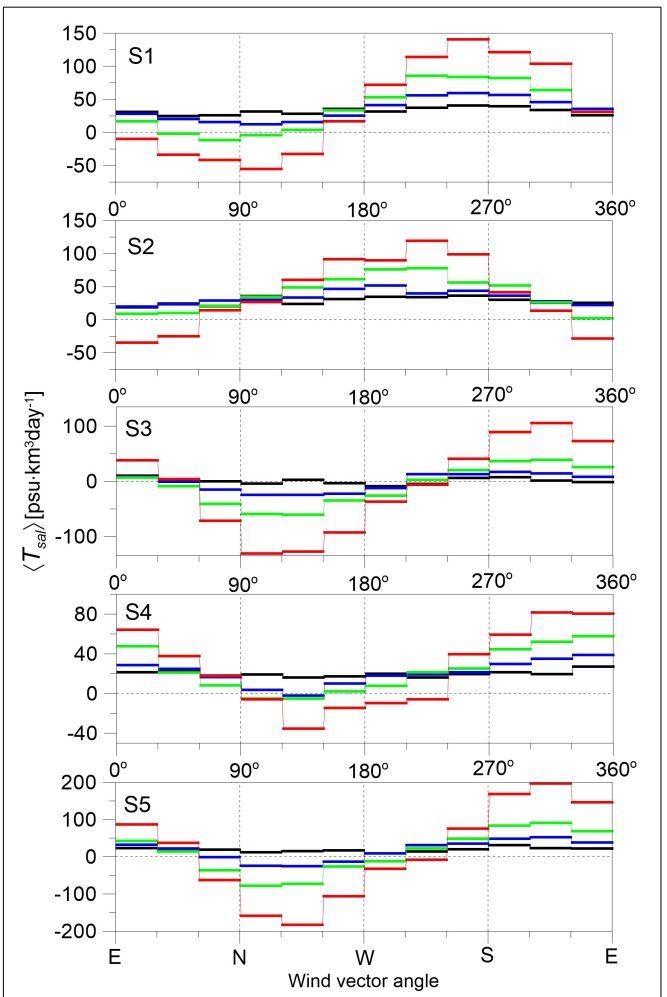

FIGURE 5 | The partial mean value $\langle T_{sal}\rangle$ of the daily saltwater transport T_{sal} through the five cross-sections S1–S5 for 12 ranges of the wind velocity vector angle and 4 ranges of the daily mean friction velocity u_* estimated from the 10-year time series. The friction velocity ranges are $0 \le u_* < 0.25$ cm · s^{-1} (light wind, $|V_{10}| \le 4$ m · s^{-1})—black segments, 0.25 cm · s^{-1} $\le u_* <$ 0.75 cm · s^{-1} (moderate wind, 4 m · s^{-1} $\le |V_{10}| <$ 7 m · s^{-1})—blue segments, 0.75 cm · s^{-1} $\le u_* <$ 1.5 cm · s^{-1} (fresh wind, 7 m · s^{-1} $\le |V_{10}| <$ 10 m · s^{-1})—green segments, $u_* \ge$ 1.5 cm · s^{-1} (storm wind, $|V_{10}| \ge$ 10 m · s^{-1})—red segments.

Dependence of $\langle T_{sal}\rangle$ on u_* and the wind vector angle for cross-sections S2, S3, S4, and S5 has the shape similar to that for S1, but the maximum positive value of $\langle T_{sal}\rangle$ is located in the wind vector angle range (150°, 270°), (270°, 360°), (300°, 360°), and (270°, 360°), respectively, and the minimum negative value is shifted approx. by 180° relative to the maximum positive value. A remarkable difference of the saltwater transport through S3 is that for vanishing wind forcing ($u_* \to 0$) the $\langle T_{sal}\rangle$ approx. vanishes too, while for the rest of cross-sections (S1, S2, S4, and S4), $\langle T_{sal}\rangle$ tends to a definitely positive value.

To learn which wind direction is most / less favorable for saltwater transport through cross-sections S1–S5, the correlation coefficient between T_{sal} and the projection of the wind stress vector $\tau_\varphi = \langle\tau_x\rangle\cos(\varphi) + \langle\tau_y\rangle\sin(\varphi)$, where φ is the angle counting counterclockwise relative to the x-axis (eastward), was calculated from the 10-year time series of daily values of T_{sal} and τ_φ (**Figure 6**). The correlation is maximum at $r_{max} =$ 0.704, 0.701, 0.739, 0.612, and 0.812 for $\varphi(r_{max}) =$ 269, 197, 316, 339, and 320° for the cross-sections S1–S5, respectively, and, evidently, is minimum $r_{min} = -r_{max}$ for the opposite wind vector direction $\varphi(r_{min}) = \varphi(r_{max}) + 180°$. The maximum correlation between T_{sal} and τ_φ was found to be relatively high, $r_{max} =$ 0.612–0.812, showing that the local wind forcing variability can be responsible for $r^2_{max} =$ 0.403–0.659 of the variance in T_{sal} time series, while the rest of T_{sal} variance is probably caused by inflow pulses which have no direct relation to the local wind variability. Like **Figure 5**, **Figure 6** confirms that the most favorable wind direction increasing saltwater transport through the cross-sections S1–S5 is when the wind vector is directed perpendicularly to the right relative to the saltwater flow. For example, the eastward saltwater flow through cross-section S1 is maximally correlated with the southward wind stress component ($\varphi(r_{max}) =$ 269°) and the northeast saltwater transport through the cross-sections S3 and S5 is maximally correlated with the southeastward wind stress component ($\varphi(r_{max}) =$ 316 and 320°, respectively). Note that the values of $\varphi(r_{max})$ are in full correspondence with rougher estimates of the wind vector angle range at which the partial mean value $\langle T_{sal}\rangle$ of the daily saltwater transport T_{sal} through the five cross-sections S1–S5 is maximum (cf. **Figures 5**, **6**).

If we take $\varphi =$ 180, 135, 225, 315, 225° for sections S1–S5, respectively, which is in correspondence with the Krauss and Brügge (1991) hypothesis on the wind-driven coastal jets at the wind direction opposite to the saltwater flow through the sections, the correlation coefficient between T_{sal} and the projection of the wind stress vector will be $r =$ 0.201, 0.376, –0.171, 0.544, –0.250. The latter values of r are considerably smaller than r_{max} except for section S4 where $r_{max} = 0.612$.

Figures 5, **6** characterize in different ways the daily saltwater transport through cross-sections S1–S5 depending on the wind vector angle which may differ much from the total (cumulative) saltwater transport through cross-sections S1–S5 depending on the wind vector angle, because the azimuthal distribution of the cumulative wind stress is strongly anisotropic with the overwhelming dominance of winds from the west-southwest (see **Figure 3**). The percentage of the positive cumulative saltwater transport through cross-sections S1–S2 for a 10-year period of 2010–2019 depending on the wind vector direction (**Figure 7**) displays an obvious similarity with the respective daily saltwater transports vs. the wind vector direction. Namely, the maximum cumulative transport, like the daily transports, takes place at wind vectors directed toward the south for cross-section S1

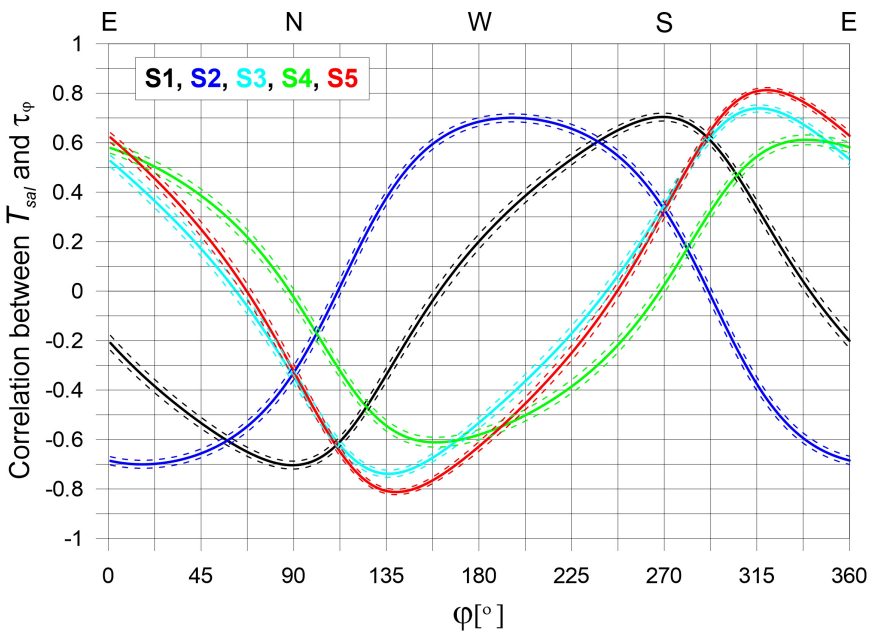

FIGURE 6 | Correlation between the daily saltwater transport T_{sal} through cross-sections S1–S5 and the projection of the wind stress vector $\tau_\varphi = \langle\tau_x\rangle\cos(\varphi) + \langle\tau_y\rangle\sin(\varphi)$ vs. angle φ. The dotted lines are the 95% confidence limits.

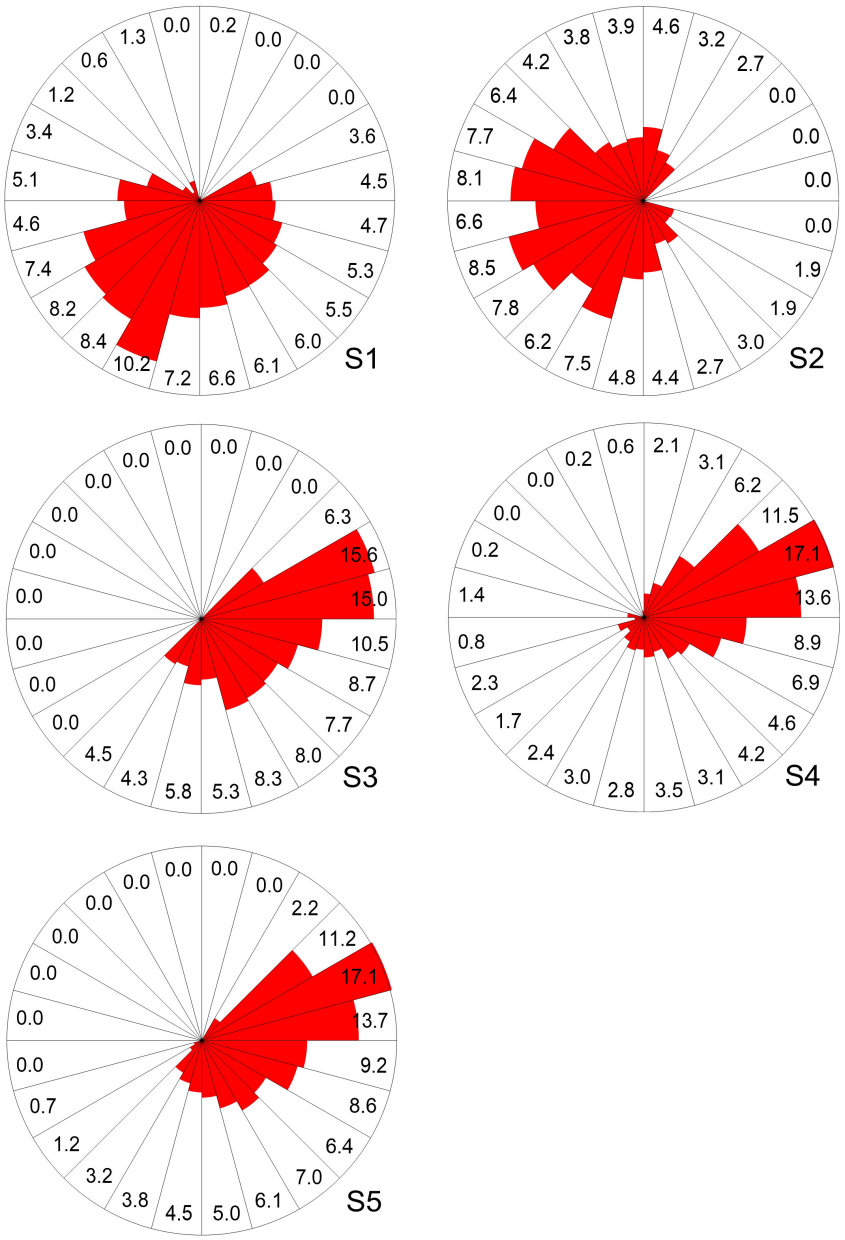

FIGURE 7 | Percentage of the positive cumulative saltwater transport through cross-sections S1–S5 for a 10-year period of 2010–2019 depending on the wind velocity vector direction.

and toward the west-southwest for cross-section S2. However, for cross-sections S3–S5 the cumulative and daily saltwater transports vs. wind vector direction behave differently. Namely, the maximum cumulative saltwater transport takes place at wind vectors directed toward east-northeast, while the maximum daily saltwater transport at wind vectors toward southeast. The discrepancy between the cumulative and daily saltwater transports vs. wind vector angle for cross-sections S3 and S5 is caused by strong anisotropy of the cumulative wind stress: The latter has a strong petal toward the east-northeast direction of the wind vector (see **Figure 3**) which provides a relatively large, positive wind stress component to the southeast favoring the saltwater transport to the north-northeast though cross-sections S3 and S5.

Correlation between daily saltwater transport T_{sal} for cross-section S1 and other four cross-sections S2–S5 is found to be positive varying between $r_{S1,S4} = 0.187$ (for cross-sections S1 and S4) and $r_{S1,S3} = 0.488$ (for cross-sections S1 and S3; **Table 1**). The positiveness of the correlation in this case can be intuitively explained by the fact that the positive fluctuation of T_{sal} through the SF (cross-section S1) leads to an increase of T_{sal} through the other cross-sections S2–S5, and the correlation will be minimal

TABLE 1 | Correlation coefficient r between daily saltwater transports T_{sal} through cross-sections S1–S5 calculated from the 10-year time series.

S1	S2	S3	S4	S5	
$r_{S1,S1} = 1$	$r_{S1,S2} = 0.394$[0.367, 0.420]	$r_{S1,S3} = 0.488$[0.464, 0.512]	$r_{S1,S4} = 0.187$[0.157, 0.218]	$r_{S1,S5} = 0.405$[0.378, 0.431]	S1
	$r_{S2,S2} = 1$	$r_{S2,S3} = -0.401$[–0.427,–0.374]	$r_{S2,S4} = -0.442$[–0.467, –0.416]	$r_{S2,S5} = -0.455$[–0.479, –0.429]	S2
		$r_{S3,S3} = 1$	$r_{S3,S4} = 0.415$[0.389, 0.441]	$r_{S3,S5} = 0.862$[0.853, 0.870]	S3
			$r_{S4,S4} = 1$	$r_{S4,S5} = 0.662$[0.644, 0.679]	S4
				$r_{S5,S5} = 1$	S5

Numbers in square brackets are the 95% confidence intervals.

for cross-sections S1 and S4, since the saltwater from the cross-section S1 reaches cross-section S4 along the longest route with an cyclonic bypass of the Gdańsk Basin.

Correlation between daily saltwater transport T_{sal} for cross-section S2 and cross-sections S3–S5 is negative varying within (–0.455, –0.401). Negative correlation in this case is quite expected because the saltwater transport to the north (south) corresponds to the positive (negative) fluctuation of T_{sal} through cross-sections S3–S5 but negative (positive) fluctuation of T_{sal} through cross-sections S2 (see **Figure 1** and the caption to it).

The fact that the saltwater transport to the north (south) corresponds to the positive (negative) fluctuation of T_{sal} through cross-sections S3–S5 causes the positive correlation between saltwater transports through pair of cross-sections S3–S4 ($r_{S3,S4} = 0.415$), S3–S5 ($r_{S3,S5} = 0.862$), and S4–S5 ($r_{S4,S5} = 0.662$). The highest correlation, $r_{S3,S5} = 0.862$, is found for daily saltwater transports through cross-sections S3 and S5, since these two cross-sections are equally oriented (from southeast to northwest), and the saltwater transport through them describes the same process of the northeast saltwater flow toward the Gotland Deep.

The mean value $\langle\langle T_{sal}\rangle\rangle$ and standard deviation σ of the daily saltwater transport T_{sal} through cross-sections S1–S5 calculated from the 10-year time series (2010–2019) of T_{sal} (**Table 2**) show that $\langle\langle T_{sal}\rangle\rangle$ for cross-section S1 is approximately equal to the sum of $\langle\langle T_{sal}\rangle\rangle$ for cross-sections S2 and S3. This is a consequence of the balanced salt water transport, namely, the salt water leaving SF for the east has only two options: it can go either to the southeast through cross-section S2 toward the Gdańsk Basin or to the northeast through cross-section S3 directly toward the Hoburg Channel and further the Gotland Deep. Similarly, the mean daily transport through cross-section S2, $\langle\langle T_{sal}\rangle\rangle = 25.50$ psu·km^3·day^{-1}, is approximately equal to that of S4 ($\langle\langle T_{sal}\rangle\rangle = 25.24$ psu·km^3·day^{-1}) which is in accordance with the long-term constancy of the salt content and anticyclonic circulation of saltwater flow in the Gdańsk Basin. However, the mean value of daily saltwater transport through cross-section S5 is definitively less than that of the cross-section S1 ($\langle\langle T_{sal}\rangle\rangle = 18.57$ and 23.95 psu·km^3·day^{-1} for S5 and S1, respectively), and the difference is probably balanced by a salinity loss due to vertical (diapycnal) mixing. An argument in favor of the role of diapycnal mixing in the balance of salt water transport though cross-sections S1 and S5 is the existence of a hotspot of diapycnal mixing in the eastern slope of the Hoburg Channel to the south of cross-section S5 caused by the effect of "bottle neck" for the northeast saltwater flow created by a topography constriction associated with the Klaipeda Bank (Paka et al., 2019; see **Figure 1**). Standard deviation σ of T_{sal} through cross-sections S1, S2, S4, and S5 is 1.7–4.1 times more than the mean value $\langle\langle T_{sal}\rangle\rangle$ which indicates the frequent alteration in the T_{sal} time series caused by the wind forcing variability. For cross-section S3, $\langle\langle T_{sal}\rangle\rangle = -3.32$ psu·km^3·day^{-1} is negative with the absolute value much smaller (practically nil) than that for the rest of the cross-sections. In view of this and recalling that the partial mean value $\langle T_{sal}\rangle$ for weak winds vanishes for cross-section S3 (see **Figure 5**), we conclude that unaffected by wind forcing, net gravity flow of saltwater leaving SF turns to the southeast toward the Gdańsk Deep and has no chance to turn to the northeast directly toward the Hoburg Channel.

TABLE 2 | Mean value $\langle\langle T_{sal}\rangle\rangle$ and standard deviation σ of the daily salt water transport T_{sal} through cross-sections S1–S5 calculated from the 10-year time series (2010 –2019) of T_{sal}.

Cross-section	$\langle\langle T_{sal}\rangle\rangle$ [psu·km^3·day^{-1}]	σ [psu·km^3·day^{-1}]
S1	23.95 ± 1.63	50.22
S2	25.50 ± 1.52	47.04
S3	–3.32 ± 1.76	54.43
S4	25.29 ± 1.39	42.86
S5	18.57 ± 2.44	75.22

Numbers next to the ± sign determine the 95% confidence intervals of $\langle\langle T_{sal}\rangle\rangle$.

DISCUSSION AND CONCLUSION

The objective of this study is to investigate the saltwater exchange between the basins of the southeastern Baltic Sea, such as the Słupsk Furrow, the Gdańsk Deep, the Hoburg Channel, and the Gotland Deep, depending on wind forcing based on numerical simulations. We hypothesized that the saltwater transport in a system of basins including the Gdańsk and Gotland deeps connected by the Hoburg Channel, is greatly controlled by wind forcing. Wind-driven Ekman transport in the upper layer directed to the south from the Gotland Deep to the Gdańsk Deep develops a compensatory saltwater countercurrent in the deep layer directed to the north from the Gdańsk Deep to the Gotland Deep, and, vice versa, the wind-driven Ekman transport directed to the north develops a compensatory saltwater flow to the south from the Gotland Deep to the Gdańsk Deep. This hypothesis is based on an analogy between the bottom topography configurations of the Bornholm Basin—SF—deep basins east of SF and the Gdańsk Deep—Hoburg

Channel—Gotland Deep and the results of numerical modeling by Krauss and Brügge (1991) showed that the saltwater transport to the east through SF is enhanced by northerly and easterly winds and weakened by southerly and westerly winds. Note that the hypothesis stating that the wind-driven Ekman transport in the upper layer drives saltwater countercurrent in the lower layer, differs from the original hypothesis by Krauss and Brügge (1991) stating that coastal jets in the wind direction drive countercurrents in the central region, deflected by bottom topography, including saltwater countercurrent in the lower layer. To our mind, both hypothesis are robust, and the results of modeling give an opportunity to resolve which effect, the wind-driven coastal jets or wind-driven Ekman transport in the open sea, prevails. If the effect of wind-driven coastal jets prevails, the maximum saltwater transport to the east through SF and to the northeast through the Hoburg Channel will take place at easterly and northeasterly winds, respectively. If the effect of wind-driven Ekman transport in the open sea prevails, the maximum saltwater transport to the east through SF and to the northeast through the Hoburg Channel will take place at northerly and northwesterly winds, respectively.

To resolve between the hypotheses, results of numerical modeling of the Baltic Sea circulation for a 10-year period 2010–2019) are applied. The model setup is based on GETM with 0.5 nautical mile grid (Zhurbas et al., 2018; Liblik et al., 2020). Validation of the model was performed by the comparison of salinity time series in the surface and bottom layers measured at the IOW monitoring station TF0256, located at the eastern exit of SF, with the simulated time series.

If the wind forcing is weak or absent, the simulated saltwater flow leaving SF for the east turns to the southeast in accordance to the gravity current dynamics and having made a cyclonic detour in the Gdańsk Basin heads north toward the Hoburg Channel and further the Gotland Deep. The mean value of the daily saltwater transport through SF, $\langle\langle T_{sal}\rangle\rangle = 23.95$ psu·km^3·day^{-1}, calculated for the 10-year simulation period, exceeds similar estimate for the Hoburg Channel, $\langle\langle T_{sal}\rangle\rangle = 18.57$ psu·km^3·day^{-1}, and the difference is probably balanced by a salinity loss due to vertical (diapycnal) mixing. An argument in favor of the role of diapycnal mixing in the balance of salt water transport though cross-sections S1 and S5 is the existence of a hotspot of diapycnal mixing in the eastern slope of the Hoburg Channel to the south of cross-section S5 caused by the effect of "bottle neck" for the northeast saltwater flow created by a topography constriction associated with the Klaipeda Bank (Paka et al., 2019).

The daily saltwater transport to the east through SF is found to be highly correlated with the wind stress component toward south (the correlation coefficient is 0.704) which is in accordance with the Krauss and Brügge (1991) findings. Even a higher correlation, $r = 0.812$, is found for the daily saltwater transport to the northeast through the Hoburg Channel (cross-section S5) and the wind stress component toward southeast, which confirm the above mentioned hypothesis on the prevalence of the effect of open-sea Ekman transport rather than that of the coastal jets. More confirmation of the hypothesis yields similar calculations for cross-sections S2 and S3: maximum correlation of $r = 701$ and 0.739 was found between the saltwater transport to the southeast and northeast and the wind stress component to the southwest and southeast for cross-sections S2 and S3, respectively. However, the rule saying that the maximum correlation between the saltwater transport through a cross-section and a wind stress component directed perpendicularly to the right relative to the direction of saltwater transport being exactly satisfied for cross-sections S1, S2, S3, and S5, is violated to some extent for cross-section S4 where the maximum correlation, $r = 0.612$, takes place for the saltwater transport to the northwest and the wind stress component toward the east (instead of the northeast in accordance to the rule). A violation of the rule in the case of cross-section S4 can be intuitively explained by a well pronounced curvature of the deep layer isobaths steering the flow caused by the proximity of the Klaipeda Bank which provides a drastic change of the saltwater flow direction nearby cross-section S4.

However, the fact that the wind velocity vector directed to the southeast is the most favorable for the saltwater transport to the northeast through the Hoburg Channel does not guarantee that the cumulative saltwater transport through cross-section S5 is maximum for the same wind velocity vector direction. Actually, the maximum cumulative saltwater transport takes place at wind velocity vectors directed toward east-northeast, while the maximum daily saltwater transport at wind velocity vectors toward southeast. The discrepancy between the cumulative and daily saltwater transports vs. wind velocity vector angle for cross-section S5 (as well as for cross-section S3) is caused by strong anisotropy of the cumulative wind stress: the latter has a strong petal toward the east-northeast direction of the wind velocity vector (see **Figure 3**) which provides a relatively large, positive wind stress component to the southeast favoring the saltwater transport to the northeast though the Hoburg Channel.

DATA AVAILABILITY STATEMENT

The raw data supporting the conclusions of this article will be made available by the authors, without undue reservation.

AUTHOR CONTRIBUTIONS

VZ proposed the idea of the work, developed the approach needed, performed statistical processing of the model output, participated in interpreting the results, and prepared the manuscript with contributions from both authors. GV developed the model setup, performed numerical modeling and primary processing of the model output, participated in interpreting the results.

FUNDING

VZ was supported by budgetary financing of the Shirshov Institute of Oceanology RAS (Project No. 149-2019-0003). GV was supported by the Estonian Research Council (grant no. PRG602).

ACKNOWLEDGMENTS

An allocation of computing resources on High Performance Computing cluster by the Tallinn University of Technology and the University of Tartu was gratefully acknowledged. The GETM community in Leibniz Institute of Baltic Sea Research (IOW) was greatly acknowledged for maintaining and developing the model code along with their user support.

REFERENCES

Borenäs, K., Hietala, R., Laanearu, J., and Lundberg, P. (2007). Some estimates of the Baltic deep-water transport through the Stolpe trench. *Tellus A* 59, 238–248. doi: 10.1111/j.1600-0870.2006.00221.x

Burchard, H., and Bolding, K. (2001). Comparative analysis of four second-moment turbulence closure models for the oceanic mixed layer. *J. Phys. Oceanogr.* 31, 1943–1968. doi: 10.1175/1520-04852001031<1943:CAOFSM<2.0.CO;2

Burchard, H., and Bolding, K. (2002). *GETM – A General Estuarine Transport Model, Scientific Documentation, Technical Report EUR 20253 EN*. Ispra: European Commission.

Canuto, V. M., Howard, A., Cheng, Y., and Dubovikov, M. S. (2001). Ocean turbulence. Part I: one-point closure model—momentum and heat vertical diffusivities. *J. Phys. Oceanogr.* 31, 1413–1426. doi: 10.1175/1520-04852001031<1413:OTPIOP<2.0.CO;2

Döös, K., Meier, H. E. M., and Döscher, R. (2004). The Baltic haline conveyor belt or the overturning circulation and mixing in the Baltic. *Ambio* 33, 261–266. doi: 10.1579/0044-7447-33.4.261

Gräwe, U., Holtermann, P., Klingbeil, K., and Burchard, H. (2015). Advantages of vertically adaptive coordinates in numerical models of stratified shelf seas. *Ocean Model.* 92, 56–68. doi: 10.1016/j.ocemod.2015.05.008

Hofmeister, R., Burchard, H., and Beckers, J. M. (2010). Non-uniform adaptive vertical grids for 3D numerical ocean models. *Ocean Model.* 33, 70–86.

Janssen, F., Schrum, C., and Backhaus, J. O. (1999). A climatological data set of temperature and salinity for the Baltic Sea and the North Sea. *Deutsche Hydrogr. Z.* 51:5. doi: 10.1007/BF02933676

Johnson, G. C., and Sanford, T. B. (1992). Secondary circulation in the Faroe Bank channel outflow. *J. Phys. Oceanogr.* 22, 927–933. doi: 10.1175/1520-04851992022<0927:SCITFB<2.0.CO;2

Klingbeil, K., Lemarié, F., Debreu, L., and Burchard, H. (2018). The numerics of hydrostatic structured-grid coastal ocean models: state of the art and future perspectives. *Ocean Model.* 125, 80–105. doi: 10.1016/j.ocemod.2018.01.007

Kondo, J. (1975). Air-sea bulk transfer coefficients in diabatic conditions. *Boundary Layer Meteorol.* 9, 91–112. doi: 10.1007/BF00232256

Krauss, W., and Brügge, B. (1991). Wind-produced water exchange between the deep basins of the Baltic Sea. *J. Phys. Oceanogr.* 21, 373–384. doi: 10.1175/1520-04851991021<0373:WPWEBT<2.0.CO;2

Large, W. G., and Pond, S. (1981). Open ocean momentum flux measurements in moderate to strong winds. *J. Phys. Oceanogr.* 11, 324–336. doi: 10.1175/1520-04851981011<0324:OOMFMI<2.0.CO;2

Liblik, T., Väli, G., Lips, I., Lilover, M.-J., Kikas, V., and Laanemets, J. (2020). The winter stratification phenomenon and its consequences in the Gulf of Finland, Baltic Sea. *Ocean Sci.* 16, 1475–1490. doi: 10.5194/os-16-1475-2020

Männik, A., and Merilain, M. (2007). Verification of different precipitation forecasts during extended winter-season in Estonia. *HIRLAM Newslett.* 52, 65–70.

Matthäus, W., and Frank, H. (1992). Characteristics of major Baltic inflows – a statistical analysis. *Cont. Shelf Res.* 12, 1375–1400. doi: 10.1016/0278-4343(92)90060-W

Mohrholz, V. (2018). Major Baltic inflow statistics – revised. *Front. Mar. Sci.* 5:384. doi: 10.3389/fmars.2018.00384

Paka, V. T., Zhurbas, V. M., Golenko, M. N., Korzh, A. O., Kondrashov, A. A., and Shchuka, S. A. (2019). Innovative closely spaced profiling and current velocity measurements in the southern Baltic Sea in 2016–2018 with special reference to the bottom layer. *Front. Earth Sci.* 7:111. doi: 10.3389/feart.2019.00111

Umlauf, L., and Burchard, H. (2005). Second-order turbulence closure models for geophysical boundary layers. A review of recent work. *Cont. Shelf Res.* 25, 795–827. doi: 10.1016/j.csr.2004.08.004

Wåhlin, A. K. (2002). Topographic steering of the dense currents with application to submarine canyons. *Deep Sea Res. I* 49, 305–320. doi: 10.1016/S0967-0637(01)00058-9

Zhurbas, V., Elken, J., Paka, V., Piechura, J., Väli, G., Chubarenko, I., et al. (2012). Structure of unsteady overflow in the Słupsk Furrow of the Baltic Sea. *J. Geophys. Res. Oceans* 117:C04027. doi: 10.1029/2011JC007284

Zhurbas, V., Elken, J., Väli, G., Kuzmina, N., and Paka, V. (2010). Pathways of suspended particles transport in the bottom layer of the southern Baltic Sea depending on the wind forcing (Numerical Simulation). *Oceanology* 50, 841–854. doi: 10.1134/S0001437010060032

Zhurbas, V., Väli, G., Golenko, M., and Paka, V. (2018). Variability of bottom friction velocity along the inflow water pathway in the Baltic Sea. *J. Mar. Syst.* 184, 50–58. doi: 10.1016/j.jmarsys.2018.04.008

Conflict of Interest: The authors declare that the research was conducted in the absence of any commercial or financial relationships that could be construed as a potential conflict of interest.

Publisher's Note: All claims expressed in this article are solely those of the authors and do not necessarily represent those of their affiliated organizations, or those of the publisher, the editors and the reviewers. Any product that may be evaluated in this article, or claim that may be made by its manufacturer, is not guaranteed or endorsed by the publisher.